A&A 559, A12 (2013)
DOI: 10.1051/0004-6361/201221012

Astronomy & Astrophysics

A study of two high-velocity red horizontal branch stars⋆,⋆⋆,⋆⋆⋆

C. B. Pereira[1], E. G. Jilinski[1,2,3], N. A. Drake[1,4], V. G. Ortega[1], and F. Roig[1]

[1] Observatório Nacional, Rua José Cristino 77, São Cristóvão, 20921-400 Rio de Janeiro-RJ, Brazil
e-mail: [claudio;jilinski;drake;vladimir;froig]@on.br
[2] Instituto de Física, Universidade do Estado do Rio de Janeiro, Rua São Francisco Xavier 524, Maracanã, 20550-900 Rio de Janeiro-RJ, Brazil
[3] Pulkovo Observatory, Russian Academy of Sciences, 65, Pulkovo, 196140 Saint Petersburg, Russia
[4] Sobolev Astronomical Institute, Saint Petersburg State University, Universitetski pr. 28, 198504 Saint Petersburg, Russia

Received 27 December 2012 / Accepted 28 July 2013

ABSTRACT

Context. High-velocity halo stars provide important information about the properties of the extreme Galactic halo. The study of Population II unbound and bound stars enables us better estimate the mass of the halo.
Aims. We carried out a detailed spectroscopic and kinematic study of two red horizontal branch stars, CD-41°15048 and HD 214362.
Methods. The atmospheric parameters, chemical abundances, and kinematical properties were determined using high-resolution optical spectroscopy and employing the local thermodynamic equilibrium model atmospheres of Kurucz and the spectral analysis code MOOG.
Results. We found that CD-41°15048 and HD 214362 are metal-poor red horizontal branch stars. Their abundance patterns are similar to other metal-poor halo stars already investigated. Our kinematic analysis of the 3D space motions shows that HD 214362 has a highly eccentric (e = 0.95) orbit and passes at 2 kpc from the Galactic center. CD-41°15048, for an adopted distance of 1.3 kpc, has an extreme retrograde motion and travels with very high velocity relative to the Galactocentric reference frame ($V_{\rm GRF}$ = 583 km s^{-1}).
Conclusions. CD-41°15048 is a bound or an unbound star, depending on the adopted Galactic potential. We also show that the red horizontal branch star BD+09°3223 is another example of a hypervelocity star. Whether it is bound or unbound to the Galaxy depends on the assumed mass and adopted Galactic potential. Possible origins of these two high-velocity stars are briefly discussed. CD-41°15048 and BD+09°3223 are further examples of evolved stars to join the restricted group of hypervelocity stars. Finally, our results seem to contradict the idea that a passage of a star very close to the Galactic center is the only possible origin of hypervelocity stars.

Key words. stars: horizontal-branch – Galaxy: kinematics and dynamics – stars: evolution

1. Introduction

Hypervelocity stars (HVSs) are stars that have space velocities higher than the Galactic escape velocity. According to Hills (1988), HVSs are a natural consequence of the presence of a massive black hole in the Galactic center. The first HVS was discovered by Brown et al. (2005): SDSS J090745.0+024507, a late B-type main-sequence star at a distance of ∼110 kpc in the Galactic halo with a radial velocity (RV) of 853±12 km s^{-1}. Following this discovery, several other HVSs and HVS candidates, the majority of them early-type main-sequence stars, were also found in subsequent surveys using the photometric filters of the Sloan Digital Sky Survey (SDSS) combined with spectroscopic observations (Brown et al. 2009). Further main-sequence HVSs were found by Li et al. (2012) using data from SDSS. These authors found other main-sequence HVSs stars, all of them metal-poor F stars. The star US 708 was the first evolved object found to be an HVS (Hirsch et al. 2005). The blue horizontal branch star SDSS J153935.67+023909.8, which is the first Population II HVS, with $V_{\rm GRF}$ ∼ 700 km s^{-1}, became one of the fastest known halo stars (Przybilla et al. 2010). The discovery that US 708 is an HVS triggered a project to search for these kinds of objects using SDSS, and Tillich et al. (2011) successfully found ten additional new subdwarf HVS candidates.

Kinematic studies of HVSs have been mainly performed solely on their RVs. This is because proper motions can be measured only for a few HVSs (Tillich et al. 2009, 2011). Therefore only stars with very high RVs are considered as potential HVSs. However, as we show in this work, a star does not need to have an extreme RV such as those quoted in Table 1 of Brown et al. (2009a), to be considered an HVS.

The metal-poor red horizontal branch (RHB) star CD-41°15048 with a RV of 229 km s^{-1} and a large proper motion is another HVS candidate depending on the adopted Galactic potential. We will see that CD-41°15048 travels with

⋆ Based on observations made with the 2.2 m telescope at the European Southern Observatory (La Silla, Chile) under the agreement between ESO and Observatório Nacional (2007–2010).
⋆⋆ Figures 3–5, 8, 10–12, Tables 1, 3, and 5 are available in electronic form at http://www.aanda.org
⋆⋆⋆ Reduced spectra for both stars (FITS files) are only available at the CDS via anonymous ftp to cdsarc.u-strasbg.fr (130.79.128.5) or via http://cdsarc.u-strasbg.fr/viz-bin/qcat?J/A+A/559/A12

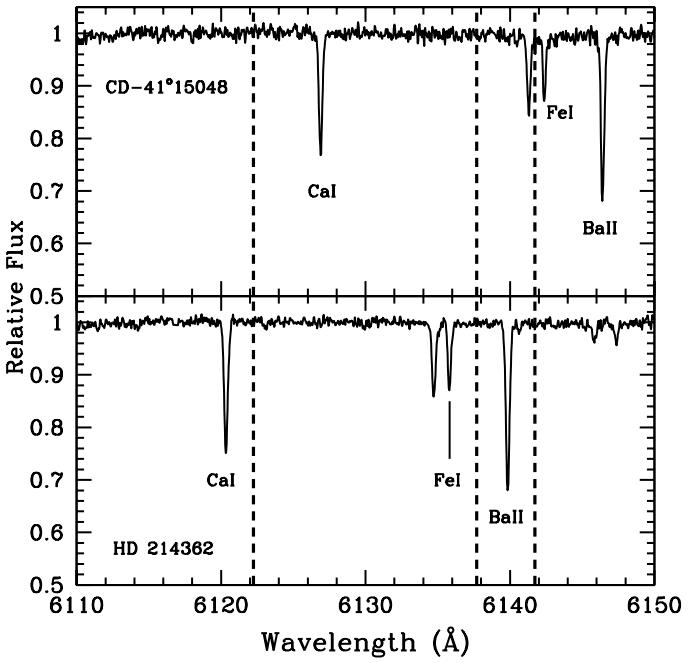

Fig. 1. Spectra of CD-41°15048 (*top*) and HD 214362 (*bottom*). Absorption lines due to the transitions of Ca I 6122.23, Fe I 6137.70, and Ba II 6141.73 are also shown. Dashed lines represent their rest wavelengths. The spectral lines are shifted towards the red by about 4.6 Å for CD-41°15048 due to a RV of 228.9 ± 0.6 km s^{-1}. For HD 214362, the absorption lines are shifted towards the blue by about 2.0 Å due to a RV of −92.4 ± 0.7 km s^{-1}.

the Galactocentric Reference Frame velocity (GRF)[1], $V_{\rm GRF}$ = 583 km s^{-1}, which is higher than the local escape velocity according to the Galactic potential of Allen & Santillan (1991) but lower than local escape velocity according to the Galactic gravitational potential of Ortega et al. (2002). We also investigate in this work the kinematic behavior of the RHB star HD 214362 and show that this star has a highly eccentric orbit and passes quite close to the Galactic center.

2. Observations

The high-resolution spectra of CD-41°15048 and HD 214362 analyzed in this work the were obtained with FEROS, the Fiber-fed extended range optical spectrograph (Kaufer et al. 1999), at the 2.2 m ESO telescope at La Silla (Chile) on the night of September 6, 2007 and August 26, 2007. The FEROS spectral resolving power is R = 48 000, corresponding to 2.2 pixels of 15 μm, and the wavelength coverage goes from 3800 Å to 9200 Å. The nominal signal-to-noise ratio (S/N) was evaluated by measuring the rms flux fluctuation in selected continuum windows, and the typical value was S/N = 100−150 after one exposure of 1200 s. The spectra were reduced with the MIDAS pipeline reduction package, which consists of the following standard steps: CCD bias correction, flatfielding, spectrum extraction, wavelength calibration, correction of barycenter velocity, and spectrum rectification. Figure 1 shows the spectra of both stars in the 6110−6150 Å region.

[1] $V_{\rm GRF}$ is the velocity of a star in the Galactocentric reference frame and is defined as $V_{\rm GRF} = \sqrt{U_0^2 + V_0^2 + W_0^2}$, where U_0, V_0, and W_0 are the star Galactocentric velocity components.

3. Analysis and results

3.1. Line selection, equivalent width measurements, and oscillator strengths

The atomic absorption lines selected in the present study are basically the same as those used in the previous study devoted to the analysis of photospheric abundances of the candidate hypervelopcity CH star CD-62°1346 (Pereira et al. 2012, hereafter Paper I). Table 1 shows the Fe I and Fe II lines employed in the analysis, the lower excitation potentials χ(eV) of the transitions, the $\log gf$ values and the measured equivalent widths W_λ. The $\log gf$ values for the Fe I and Fe II lines given in Table 1 were taken from Cohen et al. (2004) and Lambert et al. (1996).

3.2. Determination of the atmospheric parameters

The determination of stellar atmospheric parameters such as effective temperature ($T_{\rm eff}$), surface gravity ($\log g$), microturbulence (ξ), and metallicity ([Fe/H]) (we use the notation [X/H] = $\log(N_{\rm X}/N_{\rm H})_\star - \log(N_{\rm X}/N_{\rm H})_\odot$) were determined using the local thermodynamic equilibrium (LTE) model atmospheres of Kurucz (1993) and the spectral analysis code MOOG (Sneden 1973). The atmospheric parameters with their respective uncertainties were obtained in the same way as we did in Paper I. The adopted atmospheric parameters are given in Table 2. Table 2 also provides atmospheric parameter determinations derived in previous studies. Typical uncertainties of $\sigma(T_{\rm eff})$ = ±120 K, $\sigma(\log g)$ = ±0.2 dex, and $\sigma(\xi)$ = ±0.3 km s^{-1} were found.

Spectroscopic gravities of low-metallicity giants derived from ionization balance are generally lower than photometric gravities derived from stellar parallaxes or evolutionary models (Mashonkina et al. 2011; Ruchti et al. 2013; Serenelli et al. 2012). According to the recent work of Ruchti et al. (2013), the non-local thermodynamic equilibium (NLTE) correction to the spectroscopic gravity is about +0.4 dex. Besides the metallicity and surface gravity, the NLTE corrections depend on the effective temperature. In a thorough study of RHB stars in the globular cluster M15, with even lower metallicity ([Fe/H] < −2.0) than CD-41°15048, Preston et al. (2006) derived corrections to spectroscopic gravities ($\Delta \log g = \log g_{\rm phot} - \log g_{\rm spec}$) and showed that the $\Delta \log g$ value increases strongly with the decrease of the effective temperature, achieves values of about +0.4 for RHB stars with $T_{\rm eff}$ below ∼5130 K, and essentially disappears for hotter stars. The explanation for this temperature behavior of the $\log g$ correction in RHB stars is given in For & Sneden (2010). They point out that in the line-forming region of RHB stars the electron pressure rises sharply with $T_{\rm eff}$, increasing by a factor of more than 30 from the coolest RHB stars of M 15 ($T_{\rm eff}$ = 5000 K) to the warmest $T_{\rm eff}$ = 6250 K ones.

The range of effective temperatures and surface gravities of RHB stars in M15 cover well the corresponding values of CD-41°15048 and HD 214362 analyzed in our work. In its analytical form, the relation $\Delta \log g$ vs. $T_{\rm eff}$ used in the paper of For & Sneden (2010) is

$$\log g_{\rm phot} = \log g_{\rm spec} + 28.802 - 7.655 \log T_{\rm eff,spec}.$$

Using this relation, we obtained $\Delta \log g$ = +0.1 for CD-41°15048. Therefore in the present work we consider two possible corrections for the gravity of CD-41°15048, as given in For & Sneden (2010) and Ruchti et al. (2013), and draw the conclusions taking into account both corrections. We note that adopting an NLTE correction of +0.4 results in $\log g$ = 2.3. In this case, the distance to the star would be 0.7 kpc and the

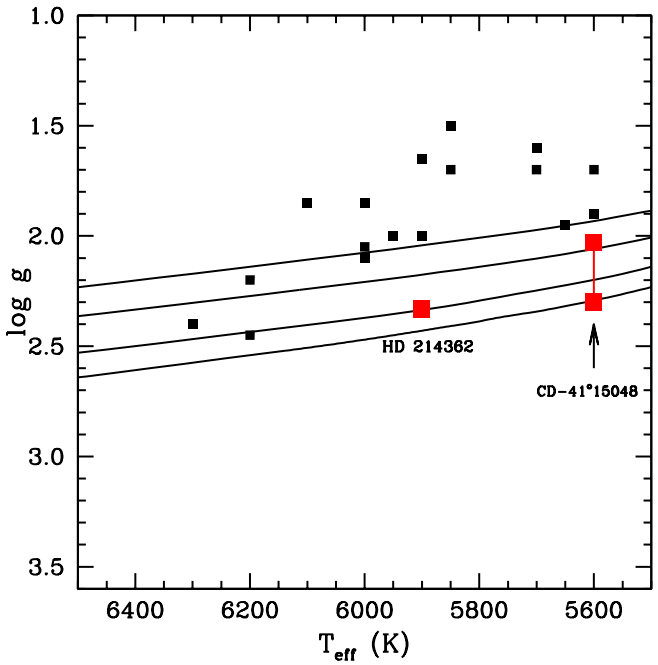

Fig. 2. Location of CD-41°15048 and HD 214362 in the $\log(T_{\rm eff}, \log g)$ plane (red squares). We also show the α-enhanced horizontal branch tracks from Pietrinferni et al. (2006) at metallicity $Z = 0.0003$ and $Y = 0.245$ for stellar masses, from top to bottom, 0.55, 0.57, 0.60, and 0.68 $M_{\odot}$. Black squares represent the positions of some RHB stars analyzed by For & Sneden (2010). For CD-41°15048 we show two possible gravities after correction.

star will not escape in any of the adopted Galactic potentials (Sects. 4.2.1 and 4.3).

For the star HD 214362, which has an even higher effective temperature, the correction to the $\log g_{\rm spec}$ disappears, and hence no correction was applied. In fact, we see that for HD 214362, the distance obtained based on the spectroscopic gravity (640 pc, Sect. 4.2.2) is inside the range of the distances given by the Hipparcos parallax, which is between 240 and 730 pc.

Having determined the temperatures and gravities of CD-41°15048 and HD 214362, we are in a position to obtain their masses using horizontal branch tracks in the $T_{\rm eff} - \log g$ plane. Because the atmospheres of the metal-poor stars are overabundant in the α-elements, we have used the evolutionary tracks computed by Pietrinferni et al. (2006) with $[\alpha/{\rm Fe}] = +0.4$. Figure 2 displays the evolutionary tracks for several stellar masses in the $T_{\rm eff} - \log g$ plane at a metallicity of $Z = 0.0003$. The positions of CD-41°15048 and HD 214362 in this plane are also shown. For CD-41°15048 we found two possible masses, depending on the adopted gravity (calculated with corrections of +0.1 and +0.4 dex), 0.57 $M_{\odot}$ or 0.68 $M_{\odot}$. For HD 214362, the mass is 0.60 $M_{\odot}$.

3.3. Abundance analysis and uncertainties

The abundances of chemical elements with their respective uncertainties were determined in the same way as in Paper I. The current version of the line-synthesis code MOOG (Sneden 1973) was used to carry out the calculations. Table 3 shows the atomic lines used to derive the abundances of the elements. We also provide the reference for the $\log gf$ values (fifth column) used in the abundance determination.

The barium abundance was derived using the Ba II lines at λ4554.0, λ4934.1, λ5853,7, and λ6141.7 Å. The line data that include hyperfine splitting were taken from McWilliam (1998). The cobalt abundance was derived using the Co I line at λ4121.33 Å, where the hyperfine splitting was taken from McWilliam et al. (1995). The europium abundance was found using the line of Eu II at λ4129.72 Å, and the hyperfine splitting was taken from Mucciarelli et al. (2008). The derived abundances are given in Table 4. The adopted abundances for the elements analyzed in this work were normalized to the solar abundances of Grevesse & Sauval (1998). For the solar iron abundance, we adopted $\log \varepsilon({\rm Fe}) = 7.52$.

The abundance uncertainties owing to errors in the stellar atmospheric parameters $T_{\rm eff}$, $\log g$, and ξ were estimated by varying these parameters by their standard errors and then computing the changes incurred in the element abundances. The abundance uncertainties owing to errors in the equivalent width measurements were computed from the expression provided by Cayrel (1988). The errors in the equivalent widths are essentially set by the signal-to-noise ratio and by the resolution of the spectra. In our case, having $R \approx 50\,000$ and a typical S/N of 150, the expected uncertainties in the equivalent widths are about 2−3 mÅ. The results of these calculations are displayed in Cols. 2 to 5 of Table 5.

4. Discussion

4.1. Abundances

Below we discuss the abundance pattern of CD-41°15048 and HD 214362 by comparing them with previous studies done for some halo population stars and also with other RHB stars. Figures 3−5 show the abundance ratios [X/Fe] versus metallicity of the elements analyzed in this work.

In metal-poor stars, the aluminum abundance was investigated by Fulbright (2000), Carretta et al. (2002), and Cohen et al. (2004), to mention just a few studies. Between [Fe/H] = −1.0 and −3.0, the [Al/Fe] ratio decreases from ≈+0.4 to ≈−0.8. In metal-poor RHB stars, aluminum is underabundant, $\langle[{\rm Al/Fe}]\rangle \approx -0.6$ (For & Sneden 2010). Our value of ≈−0.5 for the [Al/Fe] ratio for the stars CD-41°15048 and HD 214362 follows the trend observed in the metal-poor stars.

The mean α-element abundances as given by ([Mg/Fe]+[Si/Fe]+[Ca/Fe]+[Ti/Fe])/4 for CD-41°15048 and HD 214362 are, respectively, 0.36 ± 0.10 and 0.45 ± 0.05, similar for stars at this metallicity (Carretta et al. 2002; Stephens & Boesgaard 2002; Roederer 2009). For the RHB stars studied by For & Sneden (2010), the authors obtained a mean value of +0.3 for the same ratio, having a metallicity between −3.0 and −1.0.

The iron-group elements (Cr, Co, Ni, and Zn) abundances are expected to follow the iron abundance. Chromium does, indeed, and the [Cr/Fe] ratio is basically zero for both stars. Cobalt is slightly underabundant in CD-41°15048 but follows the iron abundance in HD 214362. For stars with [Fe/H] < −1.0, the [Ni/Fe] ratio starts to show a scatter around the mean [Ni/Fe] = 0.0 (Roederer 2009) larger than for stars with higher metallicity. Both RHB stars analyzed in this work have [Ni/Fe] ratios similar to those derived by Fullbright (2000), Gratton & Sneden (1991), and For & Sneden (2010).

For [Fe/H] > −1.0, the [Zn/Fe] ratio is also close to zero (Reddy et al. 2006). From the work of Cayrel et al. (2004) and Lai et al. (2008), it can be seen that the [Zn/Fe] ratio increases for metallicities down to [Fe/H] < −2.0. Between −2.0 < [Fe/H] < −1.0, the [Zn/Fe] ratio has a value around ≈+0.2, which is consistent with values found for the stars analyzed in this work.

Table 2. Atmospheric parameters of CD-41°15048 and HD 214362.

CD-41°15048					HD 214362				
$T_{\rm eff}$ (K)	$\log g$	[Fe/H]	ξ (km s^{-1})	Ref.	$T_{\rm eff}$ (K)	$\log g$	[Fe/H]	ξ (km s^{-1})	Ref.
5600	1.9	−1.98	2.2	1	5900	2.3	−1.77	2.5	1
					5727	2.6	−1.9	2.0	2
					5700	2.6	−2.2	–	3

References. (1) This work; (2) Carney et al. (2003); (3) Simmerer et al. (2004).

Table 4. Abundance in the log ε(H) = 12.0 scale and in the notation [X/Fe].

	CD-41°15048				HD 214362			
Species	n	log ε	[X/H]	[X/Fe]	n	log ε	[X/H]	[X/Fe]
Fe I	60	5.54 ± 0.11	−1.98	–	61	5.75 ± 0.11	−1.77	–
Fe II	9	5.54 ± 0.09	−1.98	–	14	5.75 ± 0.09	−1.77	–
Mg I	4	6.04 ± 0.19	−1.54	+0.44	4	6.32 ± 0.25	−1.26	+0.51
Al I	2	3.94	−2.53	−0.55	2	4.29	−2.18	−0.41
Si II	–	–	–	–	2	6.26	−1.29	+0.48
Ca I	14	4.75 ± 0.08	−1.61	+0.37	17	4.98 ± 0.09	−1.38	+0.39
Ti I	8	3.40 ± 0.15	−1.62	+0.36	13	3.67 ± 0.12	−1.35	+0.42
Ti II	11	3.23 ± 0.11	−1.79	+0.19	13	3.70 ± 0.15	−1.32	+0.45
Cr I	7	3.61 ± 0.10	−2.06	−0.08	9	3.95 ± 0.10	−1.72	+0.05
Co I	1	2.82	−2.10	−0.12	1	3.12	−1.80	+0.03
Ni I	2	4.51	−1.74	+0.24	3	4.72 ± 0.18	−1.53	+0.24
Zn I	2	2.79	−1.81	+0.17	2	3.01	−1.59	+0.18
Y II	4	0.18 ± 0.24	−2.06	−0.08	4	0.56 ± 0.23	−1.68	+0.09
Zr II	3	0.97 ± 0.14	−1.63	+0.35	4	1.28 ± 0.20	−1.32	+0.45
Ba II	3	0.34 ± 0.30	−1.79	+0.19	4	0.66 ± 0.39	−1.47	+0.30
La II	3	−0.70 ± 0.02	−1.87	+0.11	3	−0.27 ± 0.02	−1.44	+0.33
Eu II	1	−1.19	−1.70	+0.28	1	−0.79	−1.30	+0.47

Similar to the α-elements and the iron-peak elements, the elements with atomic numbers $Z > 30$ investigated in this work generally also follow a typical trend seen in halo stars. For HD 214362, we found $\log\varepsilon$(La/Eu) = 0.52 ± 0.19 in agreement with the value of 0.34 obtained by Simmerer et al. (2004). Relative to field stars in the Galaxy at similar metallicities, we did not detect any overabundances of these elements in both stars analyzed in this work. Our [X/Fe] ratios for the heavier elements are also in agreement with those obtained by For & Sneden (2010) for RHB stars.

4.2. Distance determinations

4.2.1. CD-41°15048

The relation between the star distance to the Sun r and the temperature, gravity, mass, V magnitude, and interstellar absorption (A_V) is given by

$$\log r\,(\mathrm{kpc}) = \frac{1}{2}\Big(\log\frac{M_\star}{M_\odot} + 0.4\,(V - A_V + BC) + 4\log T_{\rm eff} - \log g - 16.5\Big). \quad (1)$$

For the derived temperature and the visual magnitude, V = 10.2 [2], Eq. (1) can be written as

$$\log r\,(\mathrm{kpc}) = \frac{1}{2}\left(\log\frac{M_\star}{M_\odot} + 2.48 - \log g\right). \quad (2)$$

In these calculations, we used $M_{\rm bol\odot}$ = +4.74 (Bessel 1998) and BC = −0.19 (Alonso et al. 1999). The interstellar absorption was estimated from the relation between the equivalent width of the Na D$_2$ interstellar line and the color excess $E(B-V)$ given in Munari & Zwitter (1997). For the equivalent width of 38 mÅ, we found a color excess of 0.01. Finally, we obtain a distance r = 1.3 ± 0.3 kpc for the value of $\log g$ = 2.0, after applying a correction of +0.1 dex discussed in Sect. 3.2 and for a mass of M_* = 0.57 $M_\odot$. For the value of $\log g$ = 2.3, after applying a correction of +0.4 dex, and a mass of M_* = 0.68 $M_\odot$ we obtain a distance r = 0.7 ± 0.2 kpc. Based on the distance and interstellar absorption, we estimated the absolute visual magnitude as M_V = −0.4 ± 0.5 and M_V = 0.9 ± 0.6 for the above determined distances. These possible values for the absolute magnitudes are in the range of the M_V values of other RHB stars (e.g. the $M_V - \log T_{\rm eff}$ diagram of Simmerer et al. 2004).

There is no previous distance determination for CD-41°15048. The Hipparcos parallax for this star is very uncertain, π (mas) = 0.2 ± 1.8 (van Leeuwen 2007).

4.2.2. HD 214362

For the derived temperature and visual magnitude V = 9.1 of HD 214362, Eq. (1) can be written as

$$\log r\,(\mathrm{kpc}) = \frac{1}{2}\left(\log\frac{M_\star}{M_\odot} + 2.14 - \log g\right). \quad (3)$$

We also used the bolometric correction BC = −0.15 by Alonso et al. (1999). As for CD-41°15048, the interstellar absorption was estimated from the relation between the equivalent width of the Na D$_2$ interstellar line and the color excess. For the equivalent width of 88 mÅ, we found a color excess of 0.02. Finally, for

[2] http://simbad.u-strasbg.fr

the value of $\log g = 2.3$ and a mass of $M_* = 0.6\,M_\odot$, we obtain a distance of $r = 644 \pm 150$ pc or $\pi\,(\mathrm{mas}) = 1.55 \pm 0.37$, in good agreement with the distance given by Hipparcos (van Leeuwen 2007) ($\pi\,(\mathrm{mas}) = 2.79 \pm 1.42$), within the considered errors.

From our determined distance, we find that the absolute visual magnitude of HD 214362 is $M_V = 0.03 \pm 0.50$. This value is smaller than the one ($M_V = 0.6$) obtained by Simmerer et al. (2004). This is probably because Simmerer et al. (2004) derived a gravity higher by about +0.3 dex than our value. A higher $\log g$ value implies a smaller distance (they obtained 490 pc) and hence a higher value for the absolute visual magnitude.

4.3. Kinematics

At the distances derived in the previous section and with the RVs obtained from the spectroscopic data, we calculated the heliocentric space velocity components for the stars analyzed in this work. Table 6 shows the results. We followed the same procedure as in Paper I. A Galactocentric solar distance of 8.5 kpc and a local standard of rest (LSR) rotation velocity relative to the GRF of 220 km s^{-1} was adopted in our calculations. For CD-41°15048, we computed the space velocities considering the distances of 1.3 and 0.7 kpc. In our computations, U is positive away from the Galactic center ($l = 0°$, $b = 0°$), V is positive in the direction of the Galactic rotation ($l = 90°$, $b = 0°$), and W is positive toward the North Galactic Pole ($b = 90°$). The star escape velocity (v_{esc}) was computed using two Galactic gravitational potential models: Allen & Santillan (1991) and Ortega et al. (2002). The star escape velocity obtained from the Galactic potential is compared with the velocity (V_{GRF}) computed from the Galactocentric velocity components of the star.

The distances were calculated using Eq. (1), taking into consideration the temperature and gravity already determined. Bolometric corrections derived by Alonso et al. (1999) were also employed. Interstellar absorption was considered using the results from the literature and was not higher than $A_V = 0.3$. Proper motions were taken from Hipparcos catalogue (van Leeuwen 2007). We adopted $M_* = 0.6\,M_\odot$ for all the stars. We also included in Table 6 other RHB stars with proper motions greater than 100 mas yr^{-1}.

In the next subsections, we discuss our results for the two stars analyzed in this work and the most relevant results for the other RHB stars.

4.3.1. CD-41°15048 and HD 214362

Table 6 shows that if CD-41°15048 is at a distance of 700 pc it will be a bound object in any Galactic potential considered by us. However, for a distance of 1.3 kpc, this star may be an unbound object in the Galactic potential of Allen & Santillan (1991) but not in the Galactic potential of Ortega et al. (2002). In Fig. 6 we show the distribution probability of the Galactic reference frame velocities for CD-41°15048 for a distance of 1.3 kpc. We took into consideration the error in the RV, distance, and proper motions. Changing these three parameters with their respective errors, we applied a Monte Carlo method to obtain the distribution of space velocity components and then to obtain the Galactocentric reference frame velocities (V_{GRF}). Finally, the calculated area under the curve, which is lower-limited either by the Galactic potential of Allen & Santillan (solid vertical line) or by the Galactic potential of Ortega et al. (2002) (dashed vertical line), gives the probability of CD-41°15048 being bound or unbound. For the Galactic potential of Allen & Santillan (1991), CD-41°15048 has a 78% probability of being unbound to the Galaxy. However, according to the Galactic potential of Ortega et al. (2002), the star is bound to the Galaxy and has only a 9% probability of being unbound. As far as HD 214362 is concerned, it is a bound star in any of the Galactic potentials considered.

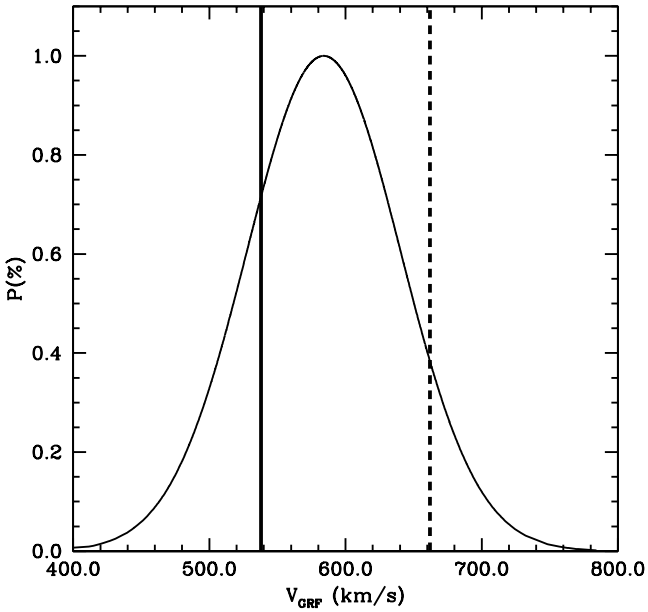

Fig. 6. Probability distribution of the Galactic reference frame velocities for CD-41°15048. The solid vertical line represents the Galactic escape velocity according to the Galactic potential of Allen & Santillan (1991), and the dashed vertical line represents the Galactic escape velocities according to the Galactic potential of Ortega et al. (2002), as given in Table 6.

4.3.2. Red horizontal branch stars analyzed with data taken from the literature: BD+09°3223 and HD 184266

Among the other RHB stars with spectroscopic data taken from the literature, two stars, BD+09°3223 (for a distance of 1.5 kpc) and HD 184266, have the highest negative values of the V_0, thus indicating retrograde motion. They also have the highest values for the Galactocentric reference frame velocity. BD+09°3223 has a Galactocentric reference frame velocity (V_{GRF}) that is very close to the escape velocity according to the Galactic potential of Ortega et al. (2002). However, it is an unbound star according to the Galactic potential of Allen & Santillan (1991), with an escape velocity of 544 km s^{-1}. The other RHB star, HD 184266, does not leave the Galaxy according to the Galactic potential of Ortega et al. (2002). However, according to the Galactic potential of Allen & Santillan (1991), with an escape velocity of 540 km s^{-1}, it almost does it. BD+09°3223, for a distance of 1.5 kpc, has an 83% probability of being unbound to the Galaxy according to the Galactic potential of Allen & Santillan (1991) and a 35% probability of being unbound to the Galaxy according to the Galactic potential of Ortega et al. (2002). All these findings show that CD-41°15048 and BD+09°3223 are the first hypervelocity RHB candidate stars. This adds those objects to the group of hypervelocity B stars first identified by Brown et al. (2005) and joins them to the other small group of hypervelocity cool stars, CD-62°1346 and HD 5223 (Paper I).

Table 6. Atmospheric parameters (effective temperature and surface gravity), distance, radial velocity (RV), proper motions, Galactocentric velocity components (U_0, V_0, W_0), Galactocentric reference frame velocity (V_{GRF}), and escape velocity (v_{esc}) in different Galactic potentials for some RHB stars.

Star	T_{eff} K	log g	Distance kpc	RV km s^{-1}	pmRA[d] mas yr^{-1}	pmDec[d] mas yr^{-1}	U_0 km s^{-1}	V_0 km s^{-1}	W_0 km s^{-1}	V_{GRF} km s^{-1}	v_{esc}[e] km s^{-1}	v_{esc}[f] km s^{-1}
CD-41°15048	5600[a]	2.0[a]	1.3	228.9[a]	38.56	−119.45	−83	−547	−184	583	662	538
	±120 K	±0.2	±0.3	±0.6	±1.0	±3.0	±4	±62	±2	±56	±0.2	±0.2
		2.3[a]	0.7				−98	−190	−189	285	661	538
		±0.2	±0.2				±3	±41	±1	±32	±0.2	±0.3
HD 214362	5900[a]	2.3[a]	0.6	−92.4[a]	173.39	−55.61	414	−79	−195	465	661	537
	±120 K	±0.2	±0.3	±0.7	±3.5	±2.9	±31	±23	±23	±40	±0.2	±0.2
BD+09°3223	5100[b]	1.3[b]	1.5	67.3[c]	−33.75	−107.17	−458	−426	−61	629	665	544
	±150 K	±0.2	±0.3	±0.2	±1.7	±2.9	±37	±63	±10	±56	±0.8	±1.5
		1.7[b]	0.9				−298	−153	−18	336	664	541
		±0.2	±0.3				±28	±47	±7	±56	±0.8	±1.7
		2.3[b]	0.2				−117	156	29	202	662	537
		±0.2	±0.05				±5	±8	±1	±12	±0.9	±0.3
BD+11°2998	5450[b]	2.3[b]	0.5	50.5[c]	−108.39	−55.13	−55	0.4	177	185	662	538
HD 25532	5450[c]	2.0[c]	0.4	−110.4[c]	91.67	−117.34	−73	−62	16	97	662	532
HD 79452	5040[c]	2.1[c]	0.1	55.8[c]	−158.20	47.73	85	248	−7	262	660	535
HD 97560	5420[c]	2.4[c]	0.3	−20.1[c]	−295.10	−114.90	299	−62	−138	335	661	534
HD 184266	5700[b]	1.7[b]	0.5	−347.5[c]	131.12	−198.13	307	−226	−349	517	662	540

Notes. For CD-41°15048, HD 214362, and BD+09°3223, we give the corresponding errors below the entries. [(a)] This work; [(b)] For & Sneden (2010); [(c)] Behr (2003); [(d)] van Leeuwen (2007); [(e)] Ortega et al. (2002); [(f)] Allen & Santillan (1991).

4.4. The orbits of CD-41°15048, HD 214362, and BD+09°3223 in the Galaxy

We also studied the dynamical orbital evolution in the Galaxy of the two RHB stars analyzed in this work and one star from the literature, BD+09°3223. We computed their orbits integrating back and forward for the two potentials considered in this work for the time interval from −2.0 to +2.0 Gyr. We integrated in time, beginning with the present distance or initial XYZ positions relative to the Sun and with current spatial velocities (UVW). As we have already mention, CD-41°15048 being at the distance of 0.7 kpc, is a bound object in any Galactic potential considered. So we show the orbits of this star for a distance of 1.3 pc. Figures 7 to 12 show the past and future orbits by considering the distance given in Table 6. The 6D position vector of the stars in the Galaxy is given by the space velocity components and their heliocentric coordinates. The velocities are given in Table 6. The Galactocentric coordinates for the three stars for which we show the orbits are $X = 7.88$ kpc, $Y = 0.05$ kpc, and $Z = -1.13$ kpc for CD-41°15048 (for an adopted distance of 1.3 kpc), $X = 8.23$ kpc, $Y = -0.18$ kpc, and $Z = -0.53$ kpc for HD 214362, and $X = 7.38$ kpc, $Y = -0.52$ kpc, and $Z = 0.87$ kpc for BD+09°3223, at a distance of 1.5 kpc.

CD-41°15048 has an orbit that goes quite high from the Galactic plane, reaching up to $Z \sim 150$ kpc, while the whole trajectory, from −2.0 Gyr to 2.0 Gyr, extends from $(X, Y) = (-55, 425)$ to $(X, Y) = (-190, -400)$. HD 214362 has a highly eccentric orbit ($e = 0.95$) and is almost unbound to the Galaxy, traveling up to 50 kpc from the Galactic plane. The orbit goes up to almost 70 kpc from the Galactic disk (in the X-axis, see Fig. 9), 80 kpc from the Galactic plane. Also, due to its high eccentricity, it passes very close to the Galactic center, at a distance of 2 kpc from it. Finally, there exists the possibility that HD 214362 could have been accelerated in the region of the Galactic bulge.

Figures 11 and 12 also show the past and future orbit of BD+09°3223 computed for both different Galactic potentials. As we have already shown, BD+09°3223 is a star bound to the Galaxy according to the Galactic potential of Ortega et al. (2002) and an unbound star according to the Galactic potential of Allen & Santillan (1991). Since some globular clusters have a high population of RHB stars, it is also probable that BD+09°3223 and CD-41°15048 could have been ejected from one of these systems. Alternatively, they could have an extragalactic origin and were captured by the Milky Way after a tidal disruption of a nearby satellite galaxy; in that case they do not belong to the Galaxy since their velocities V_{GRF} exceed the Galaxy escape velocity.

We have also verified how the uncertainty in the heliocentric distance and velocity propagates with time during the orbit integrations. We applied the same Monte Carlo procedure used in Sect. 4.3 to generate different initial orbits, taking into account the errors in distance and RV. Then each orbit was integrated backwards and forwards for ±2 Gyr using the Allen & Santillan (1991) potential, and we recorded the minimum Galactocentric distance and the corresponding time of closest approach to the Galactic center. In the case of HD 214362, the orbits registered a close approach to the Galactic center at 2.9 ± 0.1 kpc around 13.8 ± 0.6 Myr (Fig. 13). But the closest approach at 1.7 ± 0.5 kpc occurred only for the bounded orbits about 1.2 ± 0.4 Gyr in the past (Fig. 14). Moreover, bounded orbits will have another closest approach at 1.5 ± 0.5 kpc around 1.2 ± 0.4 Gyr in the future.

The approaches of the orbits of CD-41°15048 to the Galactic center are at a distance of 7.8 ± 1.9 kpc, about 3 Myr in the future. Bounded orbits of this star repeated such a close approach around 1.5 ± 0.2 Gyr in the past. The case of BD+09°3223 is

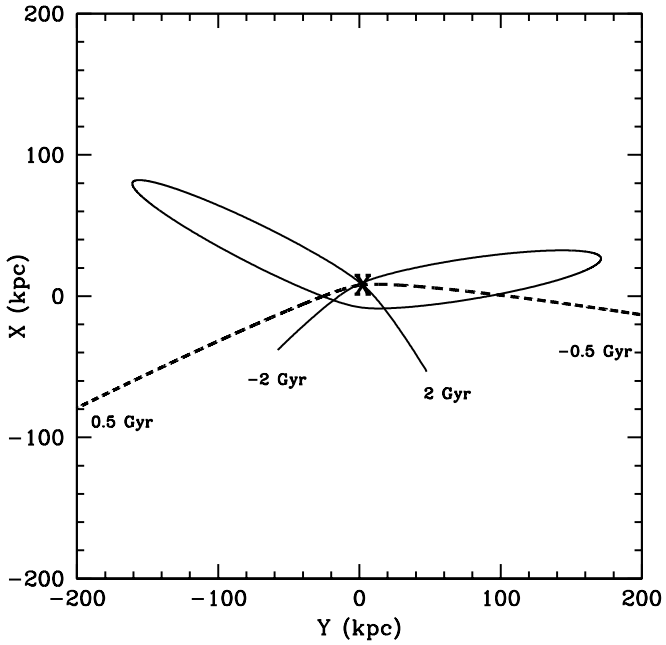

Fig. 7. Trajectory of CD-41°15048 according to the Galactic potentials of Ortega et al. (2002) (solid line) and according to the Galactic potential of Allen & Santillan (1991) (dashed line) in the XY plane. We show the whole trajectory from −2.0 Gyr to 2.0 Gyr in time for the Galactic potential of Ortega et al. (2002) while for the trajectory according to the Galactic potential of Allen & Santillan (1991) we show only a part of it from −0.5 Gyr to +0.5 Gyr. The present position is labeled with "X".

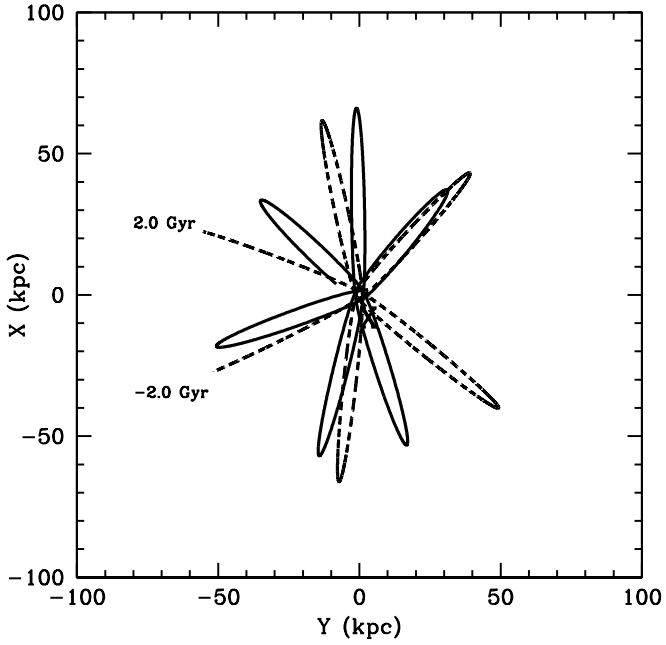

Fig. 9. Same as in Fig. 7, but for HD 214362 in the XY plane. For the Galactic potential of Ortega et al. (2002), the trajectory calculated from −2.0 Gyr to +2.0 Gyr starts and ends close to $(X, Y) = (0, 0)$. For the Galactic potential of Allen & Santillian (1991), we also show the beginning and the end of the trajectory. The present position is labeled with "X".

very similar, with a closest approach to the Galactic center at 4.3 ± 0.2 kpc, about 11 Myr in the future, and another passage at 3.7 ± 0.1 kpc, about 1.6 Gyr in the past, for the bounded orbits. Our results seem to contradict the idea of a close passage through

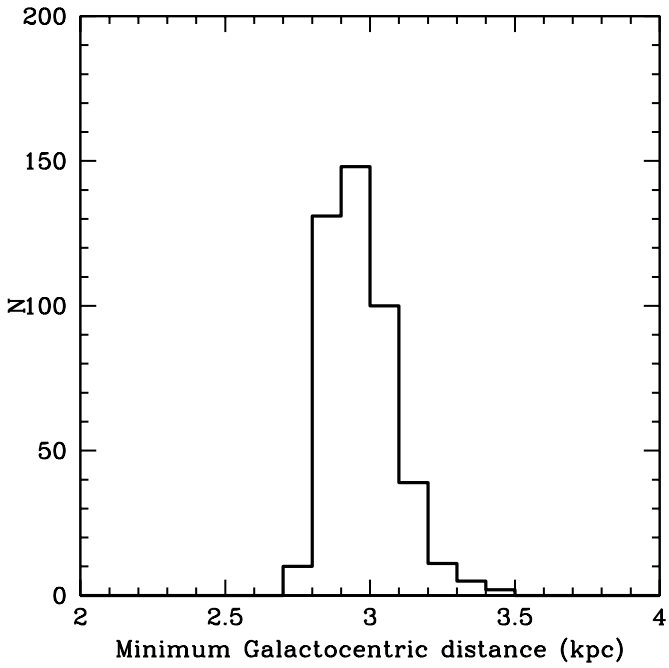

Fig. 13. Distribution of the closest approaches to the Galactic center for HD 214362 at $t \sim 14$ Myr in the past.

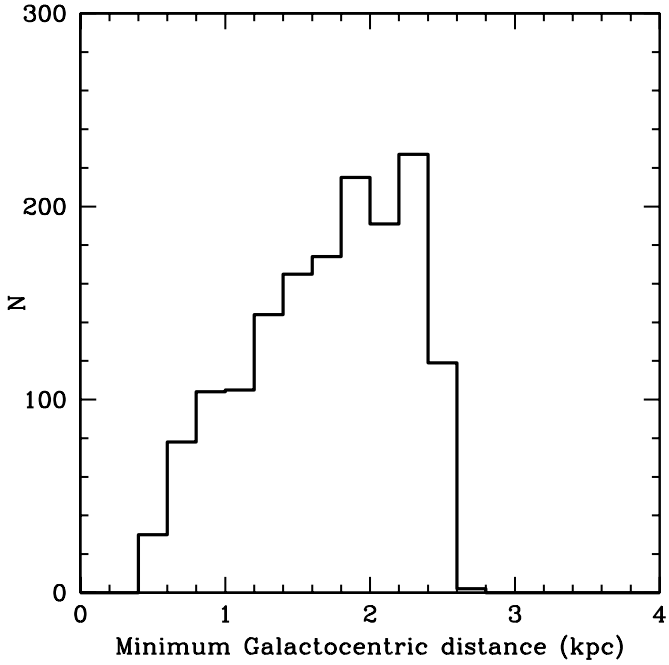

Fig. 14. Distribution of the closest approaches to the Galactic center for HD 214362 ($t = 1.2$ Gyr).

the Galactic center as the origin of the hypervelocity of these three stars.

5. Conclusions

The results of our abundance and kinematical analysis employing high-resolution optical spectra of the two RHB stars CD-41°15048 and HD 214362 can be summarized as follows:

1. CD-41°15048 is a metal-poor star ([Fe/H] = −1.98), with $T_{\rm eff}$ = 5600 K and $\log g_{\rm spec} = 1.9$. We discussed the non-LTE corrections to the spectroscopic gravity and derive the

$\log g$ value of 2.0 or 2.3 after the correction considered in Sect. 3.2. It is also a RHB star, as can be deduced from its position on the ($T_{\rm eff}$, $\log g$) diagram. CD-41°15048 and HD 214362 have abundances similar to other RHB stars previously analyzed (Simmerer et al. 2004; For & Sneden 2010).

2. If we accept a distance of 1.3 kpc, the extreme retrograde motion of CD-41°15048 ($V_0 = -546$ km s^{-1}) would suggest that it has an extragalactic origin and was captured by the Milky Way. However, the high α-element abundances, which are typical of halo stars of this metallicity, do not support this suggestion. Nissen & Schuster (2010) showed that dwarf halo stars can be distinguished according to their [α/Fe] ratios. Those with high [α/Fe] ratios would belong to the halo population, and those with low [α/Fe] ratios may have been captured from nearby galaxies. HD 214362 has a $V_{\rm GRF}$ close to the Galaxy escape velocity, making it marginally bound according to the adopted mass and hence the distance.
3. Among other RHB stars, we found that BD+09°3223 can be bound or unbound to the Galaxy, according to the Galactic potential considered.
4. Tidal disruption of a satellite galaxy or ejection from a globular cluster are good suggestions to explain the kinematical properties of CD-41°15048. However, the high α-element content of this star may provide a better explanation of the origin of this star. Since HD 214362 passes very close to the Galactic center, we cannot exclude the possibility that it has been influenced by a slingshot mechanism due to mass concentration in that region as well as the stars investigated by Tillich et al. (2011).
5. CD-41°15048 is another evolved star, in addition to the CH stars CD-62°1346 and HD 5223 (Paper I), to join the restricted group of HVSs, which formerly consisted of B-type stars only. CD-41°15048 does not have an extreme RV, as usually seen among the B-type HVSs. However, the combination of its RV of 228.9 ± 0.6 km s^{-1} and its high proper motion for a distance of 1.3 kpc makes this star another candidate for an HVS.
6. The calculations of the 3D dynamical orbits seem to contradict the idea that a passage of a star very close to the Galactic center is the only possible origin of the HVSs.

Acknowledgements. N.A.D. acknowledges the support of PCI/MCTI grant under the Project 311.868/2011-8. N.A.D. also acknowledges support of the Saint Petersburg State University, Russia, under the Project 6.38.73.2011.

References

Allen, C., & Santillan, A. 1991, Rev. Mex. Astron. Astrofis., 22, 255
Alonso, A., Arribas, S., & Martínez-Roger, C. 1999, A&A, 140, 261
Aoki, W., Honda, S., Beers, T. C., et al. 2007, ApJ, 660, 474
Beers T. C., Chiba M., Yoshii Y., et al. 2000, AJ, 119, 2866
Behr, B. B. 2003, ApJS, 149, 101
Bessell, M. S., Castelli, F., & Plez, B. 1998, A&A, 333, 231
Biemont, E., & Godefroid, M. 1980, A&A, 84, 361
Brown, W. R., Geller, M. J., Kenyon, S. J., & Kurtz, M. J. 2005, ApJ, 622, L33
Brown, W. R., & Geller, M. J., Kenyon, S. J., & Bromley, B. C. 2009a, ApJ, 690, L69
Brown, W. R., Geller, M. J., & Kenyon, S. J. 2009b, ApJ, 690, 1639
Carney, B. W., Latham, D. W., Stefanik, R. P., Laird, J. B., & Morse, J. A. 2003, AJ, 125, 293
Carretta, E., Gratton, R. Cohen, J. G., Beers, T. C., & Christlieb, N. 2002, AJ, 124, 481
Cayrel, R. 1988, Data Analysis, in The Impact of Very High S/N Spectroscopy on Stellar Physics, eds. G. Cayrel de Strobel, & M. Spite (Dordrecht: Kluwer), 345
Cayrel, R., Depagne, E., Spite, M., et al. 2004, A&A, 416, 1117
Chen, Y. Q., Zhao, G., Nissen, P. E., Bai, G. S., & Qiu, H. M. 2003, ApJ, 591, 925
Cohen, J. G., Christlieb, N., McWilliam, A., et al. 2004, ApJ, 612, 1107
Cohen, J. G., McWilliam, A., Shectman, S., et al. 2006, AJ, 132, 137
Depagne, E., Hill, V., Spite, M., et al. 2002, A&A, 390, 187
Drake, J. J., & Smith, G. 1991, MNRAS, 250, 89
Edvardsson, B., Andersen, J., Gustafsson, B., et al. 1993, A&A, 275, 101
For, Bi-Q., & Sneden, C. 2010, AJ, 140, 1694
Fulbright, J. P. 2000, AJ, 120, 1841
Gratton, R. G., & Sneden, C. 1988, A&A, 204, 193
Gratton, R. G., & Sneden, C. 1991, A&A, 241, 501
Grevesse, N., & Sauval, A. J. 1998, SSRv, 85, 161
Hills, J. G. 1988, Nature, 331, 687
Hirsch, H. A., Herber, U., O'Toole, S. J., & Bresolin, F. 2005, A&A, 444, L61
Johnson, J. A., Ivans, I. I., & Stetson, P. B. 2006, ApJ, 640, 801
Kaufer, A., Stahl, O., Tubbesing, S., et al. 1999, The Messenger, 95, 8
Kurucz, R. L. 1993, CD-ROM 13, Atlas9 Stellar Atmosphere Programs and 2 km s^{-1} Grid (Cambridge: Smithsonian Astrophys. Obs)
Lai, D. K., Bolte, M., Johnson, J. A., et al. 2008, ApJ, 681, 1524
Lambert, D. L., Heath, J. E., Lemke, M., & Drake, J. 1996, ApJS, 103, 183
Li, Y., Luo, A., Zhao, G., et al. 2012, ApJ, 744, L24
Luck, R. E., & Heiter, U. 2007, AJ, 133, 2464
Martin, W. C., Fuhr, J. R., Kelleher, D. E., et al. 2002, NIST Atomic Spectra Database Version 2.0, NIST Standard Reference Database, National Institute of Standards and Technology, Gaithersburg Maryland
Mashonkina, L., Gehren, T., Shi, J.-R., Korn, A. J., & Grupp, F. 2011, A&A, 528, A87
McWilliam, A. 1998, AJ, 115, 1640
McWilliam, A., Preston, G. W., Sneden, C., & Searle, L. 1995, AJ, 109, 275
Mishenina, T. V., Bienaymé, O., Gorbaneva, T. I., et al. 2006, A&A, 456, 1109
Mucciarelli, A., Caffau, E., Freytag, B., Ludwig, H.-G., & Bonifacio, P. 2008, A&A, 484, 841
Munari, U., & Zwitter, T. 1997, A&A, 318, 269
Nissen, P. E., & Schuster, W. J. 2010, A&A, 511, L10
Norris, J., Bessell, M. S., & Pickles, A. J. 1985, ApJS, 58, 463
Ortega, V. G., de la Reza, R., Jilinski, E., & Bazzanella, B. 2002, ApJ, 575, L75
Pereira, C. B., Jilinski, E., Drake, N. A., et al. 2012, A&A, 543, A58 (Paper I)
Pietrinferni, A., Cassisi, S., Salaris, M., & Castelli, F. 2006, ApJ, 642, 797
Preston, G. W., Sneden, C., Thompson, I. B., Shectman, S. A., & Burley, G. S. 2006, AJ, 132, 85
Przybilla, N., Tillich, A., Heber, U., & Scholz, R. D. 2010, ApJ, 718, 37
Reddy, B. E., Bakker, E. J., & Hrivnak, B. J. 1999, ApJ, 524, 831
Reddy, B. E., Tomkin, J., Lambert, D. L., & Allende Prieto, C. 2003, MNRAS, 340, 304
Reddy, B. E., Lambert, D. L., & Allende Prieto, C. 2006, MNRAS, 367, 1329
Roederer, I. U., 2009, AJ, 137, 272
Ruchti, G. R., Fulbright, J. P., Wyse, R. F. G., et al. 2011, ApJ, 737, 9
Ruchti, G. R., Bergemann, M., Serenelli, A., Casagrande, L., & Lind, K. 2013, MNRAS, 429, 126
Serenelli, A. M., Bergemann, M., Ruchti, G. R., & Casafrande, L. 2013, MNRAS, 429, 3645
Simmerer, J., Sneden, C., Cowan, J. J., et al. 2004, ApJ, 617, 1091
Smalley, B., Smith, K. C., Wonnacott, D., & Allen, C. S. 1996, MNRAS, 278, 688
Smith, G., Edvardsson, B., & Frisk, U. 1986, A&A, 165, 126
Sneden, C. 1973, Ph.D. Thesis, Univ. of Texas
Sneden, C., McWilliam, A., Preston, G. W., & Cowan, J. J. 1996, ApJ, 467, 819
Stephens, A., & Boesgaard, A. M. 2002, AJ, 123, 1647.
Tillich, A., Przybilla, N., Scholz, R.-D., & Heber, U. 2009, A&A, 507, L37
Tillich, A., Heber, U., Geier, S., et al. 2011, A&A, 527, A137
van Leeuwen, F. 2007, in Hipparcos, the New Reduction of the Raw Data, Astrophys. Space Sci. Libr., 350
van Winckel, H., & Reyniers, M., 2000, A&A, 354, 135
Venn, K. 1993, ApJ, 414, 316

Pages 9 to 14 are available in the electronic edition of the journal at http://www.aanda.org

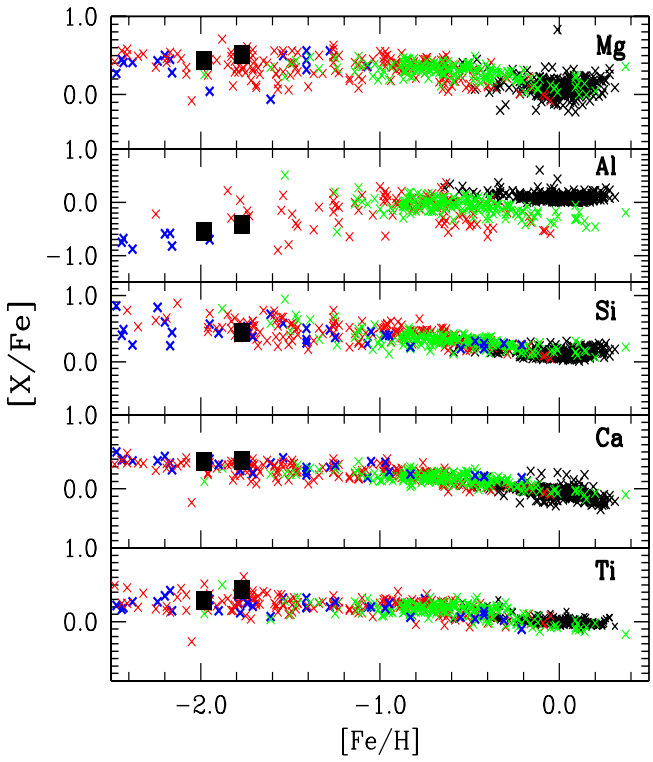

Fig. 3. Abundance ratios [X/Fe] for aluminum and α-elements versus [Fe/H]. The data were taken from Luck & Heiter (2007) (black crosses); Reddy et al. (2006) (green crosses); Fulbright (2000) (red crosses); Gratton & Sneden (1991), and For & Sneden (2011) (blue crosses). CD-41°15048 and HD 214362 are represented by black squares.

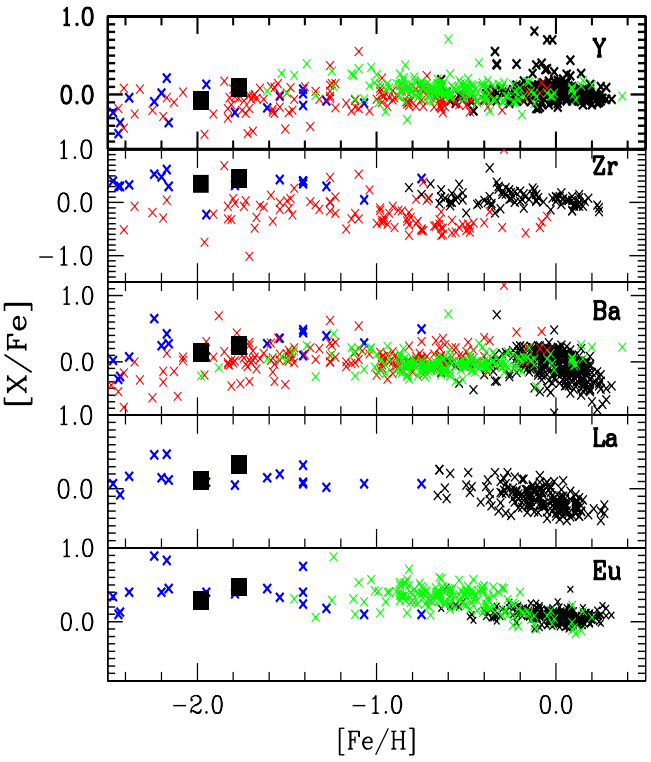

Fig. 5. Abundance ratios [X/Fe] for the heavy elements. Symbols have the same meaning as in Fig. 3, except for zirconium and lanthanum. For zirconium we used the results of Edvardsson et al. (1993) (black crosses), and for lanthanum we used the results of Mishenina et al. (2006) (black crosses).

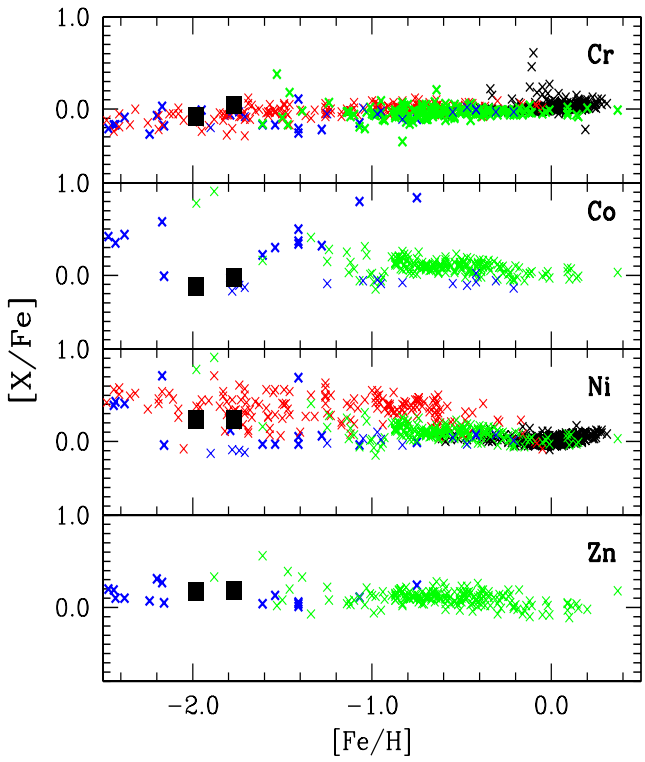

Fig. 4. Abundance ratios [X/Fe] for the iron group elements versus [Fe/H]. Symbols have the same meaning as in Fig. 3.

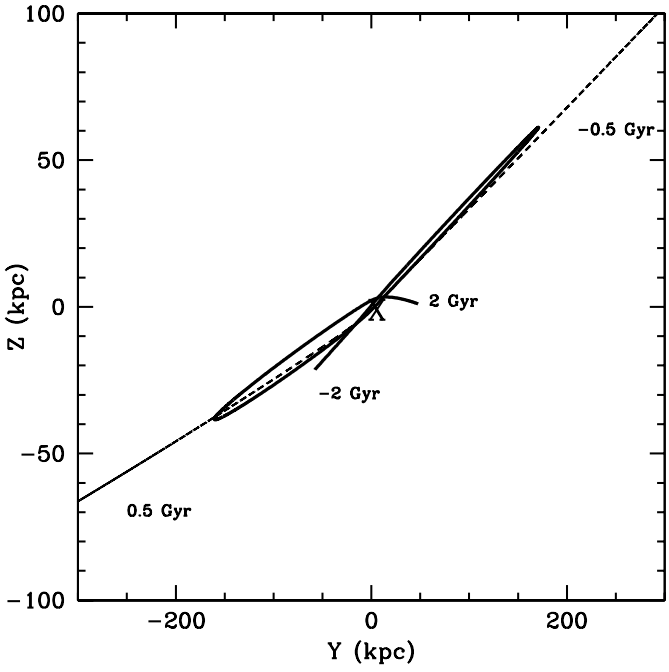

Fig. 8. Same as in Fig. 7, but in the *YZ* plane.

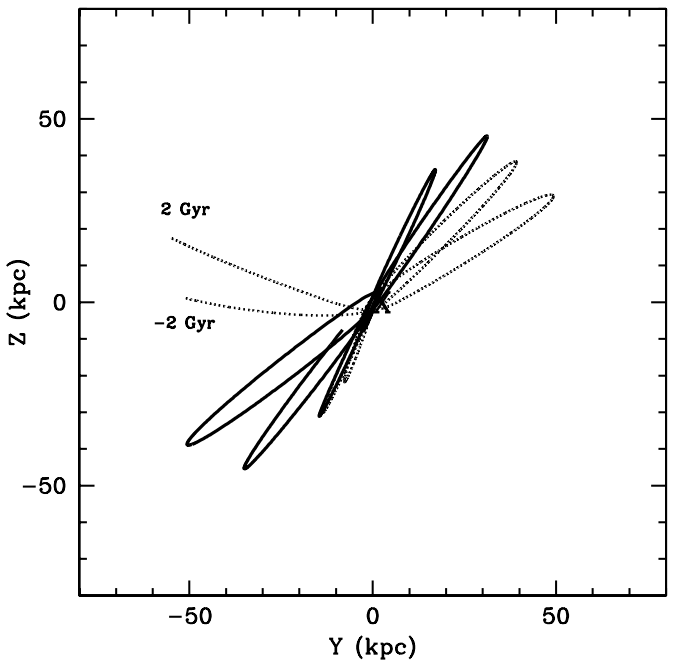

Fig. 10. Same as in Fig. 9, but in the *YZ* plane.

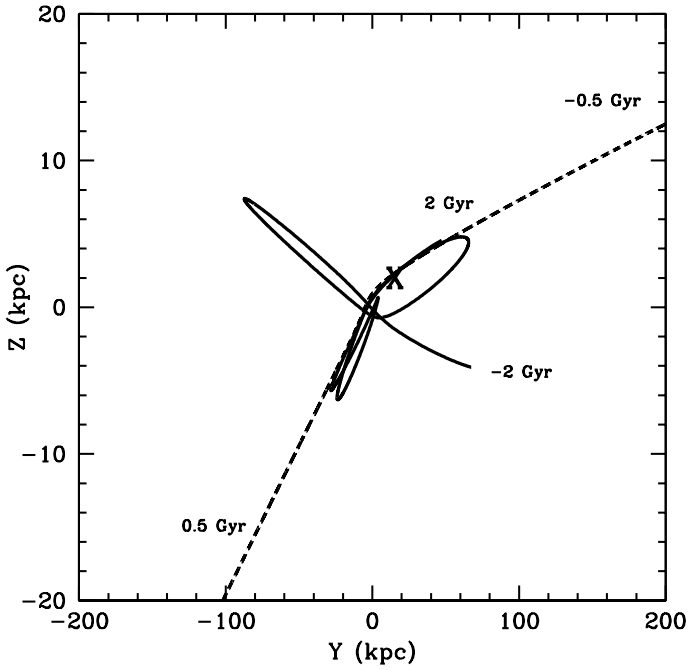

Fig. 12. Same as in Fig. 11, but in the *YZ* plane.

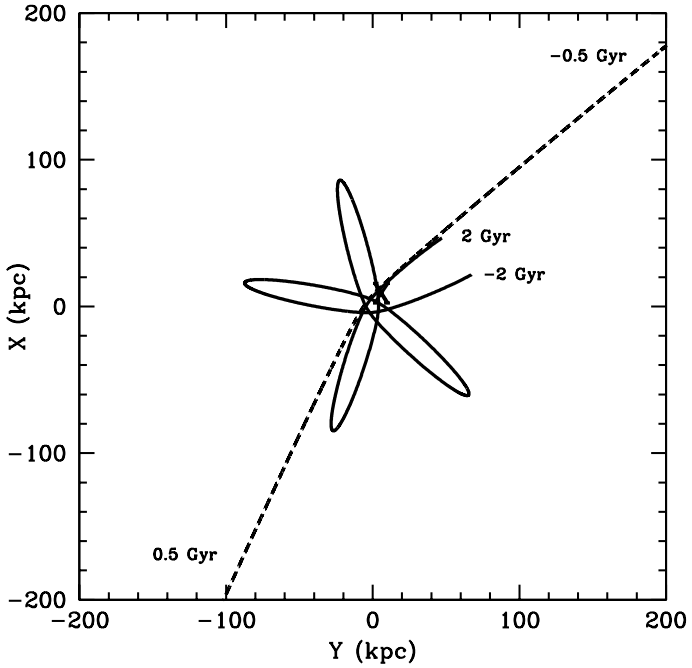

Fig. 11. Same as in Fig. 7, but for BD+09°3223 in the *XY* plane. The present position is labeled with "*X*".

Table 1. Observed Fe I and Fe II lines.

Element	λ (Å)	χ(eV)	log gf	Equivalent widths (mÅ)	
				CD-41°15048	HD 214362
Fe I	4181.75	2.83	−0.37	80	89
	4187.05	2.45	−0.55	87	92
	4187.81	2.43	−0.55	99	92
	4199.10	3.05	0.25	89	97
	4233.61	2.48	−0.60	82	–
	4250.12	2.47	−0.40	93	106
	4250.80	1.56	−0.38	127	–
	4271.15	2.45	−0.35	100	102
	4282.40	2.17	−0.82	–	93
	4427.32	0.05	−3.04	98	102
	4459.14	2.18	−1.28	72	81
	4461.65	0.09	−3.20	81	69
	4494.57	2.20	−1.14	74	73
	4531.16	1.49	−2.15	57	50
	4871.33	2.86	−0.36	75	82
	4872.14	2.88	−0.57	72	65
	4891.50	2.85	−0.11	–	97
	4920.51	2.83	+0.15	105	119
	5110.41	0.00	−3.76	58	–
	5123.72	1.01	−3.07	36	34
	5125.12	4.22	−0.08	26	31
	5133.69	4.18	+0.20	46	45
	5150.84	0.99	−3.00	29	28
	5151.91	1.01	−3.32	22	20
	5162.27	4.18	+0.07	39	38
	5171.60	1.49	−1.76	84	83
	5194.94	1.56	−2.09	66	56
	5198.71	2.22	−2.14	26	22
	5202.34	2.18	−1.84	–	38
	5232.94	2.94	−0.08	82	94
	5242.49	3.63	−0.97	–	13
	5281.79	3.04	−0.83	41	39
	5302.31	3.28	−0.74	32	32
	5307.36	1.61	−2.97	–	14
	5339.93	3.27	−0.68	39	39
	5341.02	1.61	−1.95	66	69
	5353.37	4.10	−0.68	15	16
	5364.87	4.45	+0.23	36	29
	5367.47	4.42	+0.43	33	40
	5369.96	4.37	+0.54	37	39
	5371.49	0.96	−1.65	127	–
	5393.17	3.24	−0.72	36	37
	5400.50	4.37	−0.10	–	20
	5405.77	0.99	−1.85	108	114
	5410.91	4.47	+0.40	29	30
	5434.52	1.01	−2.12	94	95
	5445.04	4.39	+0.04	23	28
	5446.92	0.99	−1.91	109	114
	5497.52	1.01	−2.84	47	38
	5506.78	0.99	−2.80	51	–
	5569.62	3.42	−0.49	36	34
	5572.84	3.40	−0.28	–	51
	5576.09	3.43	−0.85	23	27
	5658.82	3.40	−0.81	31	–
	5762.99	4.21	−0.41	19	17
	5934.65	3.93	−1.02	–	11
	6065.48	2.61	−1.53	32	29
	6136.61	2.45	−1.40	43	46
	6137.69	2.59	−1.40	30	37
	6191.56	2.43	−1.42	44	45
	6230.72	2.56	−1.28	49	44
	6252.56	2.40	−1.72	32	31
	6265.13	2.18	−2.55	16	–

Notes. The log gf values were taken from Cohen et al. (2004) and Lambert et al. (1996).

Table 1. continued.

Element	λ (Å)	χ(eV)	log gf	Equivalent widths (mÅ)	
				CD-41°15048	HD 214362
	6393.60	2.43	−1.43	39	37
	6411.65	3.65	−0.66	20	–
	6421.35	2.28	−2.01	26	29
	6430.85	2.18	−2.01	32	30
	6592.91	2.72	−1.47	33	23
Fe II	4233.17	2.58	−1.90	–	126
	4508.29	2.86	−2.25	78	84
	4515.34	2.84	−2.45	70	72
	4555.89	2.82	−2.17	79	103
	4583.84	2.81	−1.80	110	115
	5234.62	3.22	−2.24	64	71
	5284.10	2.89	−3.01	–	36
	5325.56	3.22	−3.17	15	19
	5425.25	3.20	−3.21	–	18
	5534.83	3.25	−2.77	26	30
	6149.25	3.89	−2.72	–	11
	6247.55	3.89	−2.34	21	22
	6416.92	3.89	−2.68	–	10
	6432.68	2.89	−3.58	19	12

Table 3. Other lines studied.

λ (Å)	Species	χ (eV)	log gf	Ref.	Equivalent widths (mÅ)	
					CD-41°15048	HD 214362
4057.52	Mg I	4.34	−1.20	4	49	72
4702.99	Mg I	4.35	−0.52	1	84	99
5528.42	Mg I	4.34	−0.36	10	84	92
5711.10	Mg I	4.34	−1.75	13	–	38
3944.01	Al I	0.00	−0.64	3	120	139
3961.52	Al I	0.00	−0.34	3	124	132
6347.11	Si II	8.12	+0.26	15	–	29
6371.37	Si II	8.12	−0.06	15	–	14
4425.44	Ca I	1.88	−0.36	4	57	63
4435.69	Ca I	1.89	−0.52	4	–	58
4454.79	Ca I	1.90	+0.26	4	94	111
4578.56	Ca I	2.52	−0.56	4	–	17
5581.80	Ca I	2.52	−0.67	5	20	23
5601.29	Ca I	2.52	−0.52	5	–	22
5857.46	Ca I	2.93	+0.11	5	35	–
6102.73	Ca I	1.88	−0.79	6	37	40
6122.23	Ca I	1.89	−0.32	6	69	83
6162.18	Ca I	1.90	−0.09	6	84	100
6169.04	Ca I	2.52	−0.80	14	15	15
6169.56	Ca I	2.53	−0.48	7	24	27
6439.08	Ca I	2.52	+0.47	6	71	79
6449.82	Ca I	2.52	−0.50	5	27	27
6471.66	Ca I	2.51	−0.69	16	16	21
6493.79	Ca I	2.52	−0.11	7	41	52
6499.65	Ca I	2.52	−0.81	5	18	21
6717.69	Ca I	2.71	−0.52	5	–	17
4512.74	Ti I	0.84	−0.48	12	13	17
4518.03	Ti I	0.83	−0.32	12	–	11
4533.25	Ti I	0.85	+0.48	12	43	51
4534.78	Ti I	0.84	+0.28	12	36	40
4548.77	Ti I	0.83	−0.35	12	17	22
4617.28	Ti I	1.75	+0.39	12	–	12
4681.92	Ti I	0.05	−1.07	12	–	14
4981.74	Ti I	0.85	+0.50	12	–	54
4999.51	Ti I	0.83	+0.25	4	42	–
5016.17	Ti I	0.85	−0.57	12	–	10
5022.87	Ti I	0.83	−0.43	12	21	15
5039.96	Ti I	0.02	−1.13	12	–	19
5173.75	Ti I	0.00	−1.12	12	25	16
5210.39	Ti I	0.05	−0.88	12	20	23
4399.78	Ti II	1.24	−1.27	3	93	118
4417.72	Ti II	1.17	−1.43	3	–	115
4450.49	Ti II	1.08	−1.45	11	90	110
4583.41	Ti II	1.16	−2.87	4	17	18
4589.95	Ti II	1.24	−1.65	3	75	86
4779.99	Ti II	2.05	−1.37	19	46	49
4798.52	Ti II	1.08	−2.67	3	22	36
4805.09	Ti II	2.06	−0.96	15	53	71
5154.03	Ti II	1.57	−1.92	15	40	52
5185.91	Ti II	1.89	−1.46	3	41	53
5188.70	Ti II	1.58	−1.21	11	–	114
5211.54	Ti II	2.59	−1.85	18	–	16
5336.79	Ti II	1.58	−1.70	11	50	57
5381.01	Ti II	1.57	−2.08	11	32	–

References. (1) Aoki et al. (2007); (2) Biemont & Godefroid (1980); (3) Cohen et al. (2004); (4) Cohen et al. (2006); (5) Chen et al. (2003); (6) Depagne et al. (2002); (7) Drake & Smith (1991); (8) Edvardsson et al. (1993); (9) Gratton & Sneden (1988); (10) Johnson et. al. (2006); (11) McWilliam et al. (1995); (12) Martin et al. (2002); (13) Reddy et al. (1999); (14) Reddy et al. (2003); (15) Smalley et al. (1996); (16) Smith et al. (1986); (17) Sneden et al. (1996); (18) van Winckel & Reyniers (2000); (19) Venn (1993).

Table 3. continued.

λ (Å)	Species	χ (eV)	log gf	Ref.	Equivalent widths (mÅ)	
					CD-41°15048	HD 214362
4254.35	Cr I	0.00	−0.11	11	–	127
4274.81	Cr I	0.00	−0.23	11	115	128
4289.73	Cr I	0.00	−0.36	11	–	118
5206.04	Cr I	0.94	+0.02	11	80	92
5296.70	Cr I	0.98	−1.39	9	13	12
5298.28	Cr I	0.98	−1.10	12	22	23
5345.81	Cr I	1.00	−0.98	9	22	27
5348.32	Cr I	1.00	−1.29	9	11	13
5409.79	Cr I	1.03	−0.72	9	32	33
4904.42	Ni I	3.54	−0.17	12	15	12
5084.11	Ni I	3.68	−0.18	8	15	15
5115.40	Ni I	3.83	−0.28	14	–	12
4722.16	Zn I	4.03	−0.39	2	19	18
4810.54	Zn I	4.08	−0.17	2	20	23
4374.94	Y II	0.41	+0.16	11	94	105
4883.68	Y II	1.08	+0.07	17	28	40
5087.43	Y II	1.08	−0.17	17	17	19
5205.72	Y II	1.03	−0.34	17	19	21
4161.21	Zr II	0.71	−0.72	17	27	35
4208.99	Zr II	0.71	−0.46	17	32	27
4317.32	Zr II	0.71	−1.38	17	10	11
4496.97	Zr II	0.71	−0.59	17	–	35
4086.71	La II	0.00	−0.16	17	18	22
4123.22	La II	0.32	+0.13	4	18	22
4333.75	La II	0.17	−0.06	3	17	22

Table 5. Abundance uncertainties for CD-41°15048.

Species	$\Delta T_{\rm eff}$ +120 K	$\Delta \log g$ +0.2	$\Delta\xi$ +0.3 km s^{-1}	ΔW_λ +3 mÅ	$\left(\sum \sigma^2\right)^{1/2}$	$\sigma_{\rm obs}$
Fe I	+0.11	0.00	−0.04	+0.07	0.14	0.11
Fe II	+0.03	+0.12	−0.04	+0.08	0.15	0.09
Mg I	+0.05	+0.00	−0.05	+0.05	0.09	0.19
Al I	+0.10	−0.01	−0.18	+0.08	0.22	–
Ca I	+0.07	−0.01	−0.04	+0.06	0.10	0.08
Ti I	+0.12	−0.01	−0.01	+0.07	0.14	0.15
Ti II	+0.05	+0.10	−0.04	+0.05	0.13	0.09
Cr I	+0.12	−0.01	−0.05	+0.08	0.15	0.10
Co I	+0.10	0.00	−0.05	–	0.06	–
Ni I	+0.08	+0.00	−0.01	+0.10	0.13	–
Zn I	+0.08	+0.01	−0.01	+0.07	0.11	–
Y II	+0.06	+0.10	−0.04	+0.08	0.15	0.24
Zr II	+0.04	+0.07	−0.02	+0.08	0.12	0.14
Ba II	+0.09	+0.14	+0.01	–	0.17	0.30
La II	+0.08	+0.09	−0.01	+0.08	0.14	0.02
Eu II	−0.10	−0.14	0.00	–	0.12	–

Notes. The second column gives the variation of the abundance caused by the variation in $T_{\rm eff}$. The other columns refer to the abundance variations caused by the uncertainties in log g, ξ, and W_λ, respectively. The sixth column gives the compounded rms uncertainty of the second to fifth columns. The last column gives the observed abundance dispersion for those elements whose abundances were derived using more than three lines.